J. Fluid Mech. (1992), *vol.* 239, *pp.* 383–408
Printed in Great Britain

Liquid-metal flows induced by low-frequency alternating magnetic fields

By J. M. GALPIN† AND Y. FAUTRELLE
INPG-MADYLAM, B.P. 95X, 38402 Saint Martin d'Hères Cedex, France

(Received 15 January 1990 and in revised form 8 January 1992)

This paper describes an experimental study of the influence of a low-frequency alternating magnetic field on a liquid-metal pool with a free surface. A 200 mm cylinder containing mercury is located in a solenoidal coil supplied with a single phase a.c. current of frequency 2–20 Hz. It is shown that, in that frequency range, the motion may be split into two parts: (i) a bulk motion driven by the mean Lorentz forces; (ii) a surface wave motion driven by the alternating part of the Lorentz forces.

The turbulent bulk flow is quite similar to those observed in previous electromagnetic stirring experiments at higher frequency. The peculiar feature, observed here, is the rapid decay of the mean characteristic velocity. That phenomenon seems to be related to the presence of fluctuating velocities forced by the alternating electromagnetic force.

The alternating part of the Lorentz forces is globally responsible for a surface motion whose pattern and amplitude depend on the applied electric current I and its frequency f. The (I,f)-parameter space may be split into four regions corresponding to four regimes, namely (i) concentric harmonic standing waves driven by the Lorentz forces, (ii) harmonic azimuthal waves, (iii) strong-amplitude subharmonic azimuthal waves, (iv) chaotic free-surface motion. The wave motion becomes negligible when the frequency is greater than 10 Hz.

1. Introduction

Alternating magnetic fields are commonly used in metallurgy to act on a liquid metal. The electric currents induced by an external a.c. field interact with it to create electromagnetic forces. These forces are responsible for both a vigorous motion of the bath and free-surface deformations. Single-phase magnetic fields are commonly used in various processes such as levitation, induction furnaces, continuous casting, ladle metallurgy etc.

In ladle metallurgy, electromagnetic stirring has some important advantages with respect to other techniques such as gas bubbling. Indeed, this process is robust and avoids any contact with the liquid metal. However, its efficiency is questionable especially for large ladles. Industrial supply frequencies ($\sim$ 50 Hz) are no longer well suited because of the skin effect, and lower frequencies must be used.

The use of low-frequency single-phase alternating magnetic fields exhibits some peculiar phenomena. First of all, let us define the conditions corresponding to the so-called low-frequency case which will be considered hereafter. Electromagnetically, such a regime is characterized by small values of the shield parameter R_ω such that

$$R_\omega = \mu\sigma\omega a^2, \quad \omega = 2\pi f, \tag{1}$$

† Present address: IRSID, Station d'Essais, 57210 Maizières-les-Metz, France.

$\mu, \sigma, \omega, f, a$ being respectively the magnetic permeability, the electrical conductivity, the frequency and the inverse period of the magnetic field, and the radius of the pool. In the limit of small values of R_ω, the mean part of the Lorentz forces are $O(R_\omega^2)$ at lowest order whilst the alternating one decreases like $O(R_\omega)$ (cf. Taberlet & Fautrelle 1985). In that case the pulsating part of the Lorentz force becomes predominant with respect to the mean one. Practically, it turns out that this limit holds when $R_\omega \leqslant 1$. This phenomenon has been observed by Dahlberg (1972) in the similar rotating field problem. This has been also checked by numerical calculations detailed in Appendix A. Regarding the motion, the alternating electromagnetic forces have a significant dynamical effect only if their strength is sufficient to balance the inertia of the fluid. This condition involves both the magnetic field strength and the frequency via an interaction parameter N which is an estimate of the ratio between Lorentz forces and inertia, namely

$$N = \frac{\sigma B_0^2}{\rho \omega}, \tag{2}$$

B_0, ρ respectively being the characteristic magnetic field strength and the density. As we shall see later, the oscillating vorticity becomes non-negligible when the interaction parameter N is of order of unity. The effects of a single-phase alternating field on a coreless liquid metal have been studied by many authors, both theoretically and experimentally (Tarapore & Evans 1976; Mikelson, Yakovich & Pavlov 1978; Sneyd 1971, 1979; Hunt & Maxey 1980; Moreau 1980; Fautrelle 1981; Moore & Hunt 1983; Trakas, Tabeling & Chabrerie 1984; Moffatt 1984; El Kaddah *et al.* 1986; Taberlet & Fautrelle 1985; Davidson, Hunt & Moros 1988. The previous works deal with intermediate frequencies ranging from 50 to 10 kHz. The corresponding shield parameter R_ω varies between 3 and a few hundred. In that frequency range, the liquid-metal inertia is too large to be sensitive to the alternating electromagnetic forces, and only the mean part of the Lorentz forces is taken into account. The mean Lorentz forces are responsible for a turbulent motion which entails a mean motion and turbulent fluctuations. In axisymmetric geometries, the mean flow pattern generally consists of several vortices whose number and size depend on the applied magnetic field distribution. In the well-known induction-furnace-like geometry, the flow configuration consists of two counter-rotating vortices in a meridian plane. Turbulence characteristics are similar to those of classical turbulent shear flows even when the electromagnetic skin depth is small compared with the dimension of the bath.

Little attention has been paid to the low-frequency case and the effect of the alternating part of the Lorentz force. Using rapid distortion theory Hunt & Maxey (1980) have analysed the possible effects of that force on the liquid bulk. They have shown that no resonant forcing of turbulent eddies occurs, even if the electromagnetic force fluctuations have a timescale of the same order as the turnover time of the turbulent eddies. They also gave estimates of the magnitude of the fluctuating velocities, but those relationships are restricted to the medium frequency range ($R_\omega \geqslant 1$). However, no experiments have been achieved to confirm those predictions. Galpin, Fautrelle & Sneyd (1992, hereinafter referred to as GFS) have studied theoretically the influence of a uniform alternating magnetic field on the free surface of a liquid-metal pool in the very low-frequency limit. In that case, the Lorentz forces are purely oscillating and irrotational at lowest order. Their effects are twofold; (i) they generate a system of forced standing axisymmetric waves of frequency $2f$, (ii) they are responsible for a parametric-type instability.

The work presented hereafter was intended to investigate experimentally the influence of the alternating electromagnetic forces on a liquid metal pool in a geometry similar to that of an induction furnace. The frequency varies from 2 to 22 Hz, corresponding to shield parameter values from 0.15 to 1.5.

Before detailing the various phenomena observed, it is useful to recall some features of the electromagnetic force in the axisymmetric geometry. Some details are given in Appendix A. The electromagnetic forces $\boldsymbol{j}\times\boldsymbol{B}$ are calculated from the poloidal magnetic field $\boldsymbol{B}$ and the single azimuthal component of the electrical current density $\boldsymbol{j}$. The Lorentz forces entail a mean part and an alternating part which oscillates with the frequency $2f$. The alternating part is irrotational in the bidimensional case (Sneyd 1979). It is also irrotational if $\boldsymbol{B}$ is independent of z. In the general case, it is rotational and leads to two kinds of distinct phenomena.

The mean part of the Lorentz forces drives a mean recirculating turbulent motion whose amplitude is usually quantified by the Alfvén speed u_A obtained from B_0 as follows;

$$u_A = B_0/(\mu\rho)^{\frac{1}{2}}, \tag{3}$$

μ being the magnetic permeability. The characteristic mean velocity is a percentage of the Alfvén speed which depends on the frequency of the applied currents.

The alternating electromagnetic force generates a fluctuating velocity in the liquid bulk. An estimate of the corresponding fluctuating vorticity may be obtained from the vorticity equation. Balancing inertia and the alternating electromagnetic body force in (A 6) yields an estimate of the fluctuating vorticity $\tilde{\omega}$, namely:

$$\tilde{\omega}/\omega = O(N),$$

N being the interaction parameter defined in (2).

Furthermore, the alternating force interacts with the pool free surface to create a wide variety of surface motions. To obtain an estimate of the amplitude of the forced waves, let us consider the nth free mode of surface oscillation whose eigenfrequency and amplitude respectively are $f_n = \omega_n/2\pi$, η_n. Its wavelength l_n is of order of g/ω_n^2 (see for example Lamb 1932). Following the analysis of GFS, we may assume that the largest-amplitude mode is the one which is the nearest to the resonance, i.e. $\omega_n = O(\omega)$. It follows that the wavelength of the largest-amplitude mode is such that:

$$l_n = O(g/\omega^2). \tag{4}$$

For small magnetic field values, the order of magnitude of η_n is obtained from a balance between the gravity and the electromagnetic forces. Using l_n as the relevant length scale in the Lorentz force, η_n is estimated as

$$\frac{\eta_n}{a} = O\left(\frac{\sigma B_0^2}{\rho\omega}\frac{l_n}{a}\right) = O(N/F^2), \tag{5}$$

with $F = (a\omega^2/g)^{\frac{1}{2}}$. For large magnetic field values, an estimate of the wave amplitude η_n may be obtained from the balance between inertia and the Lorentz forces. Assuming that the corresponding velocity is of order of $\omega\eta_n$, the order of magnitude of η_n is

$$\frac{\eta_n}{a} = O\left(\frac{\sigma B_0^2 g^2}{\rho\omega^5 a^2}\right)^{\frac{1}{3}} = O\left(\frac{N^{\frac{1}{3}}}{F^2}\right). \tag{6}$$

Relations (5) and (6) illustrate the importance of the parameter N. Note that (5)

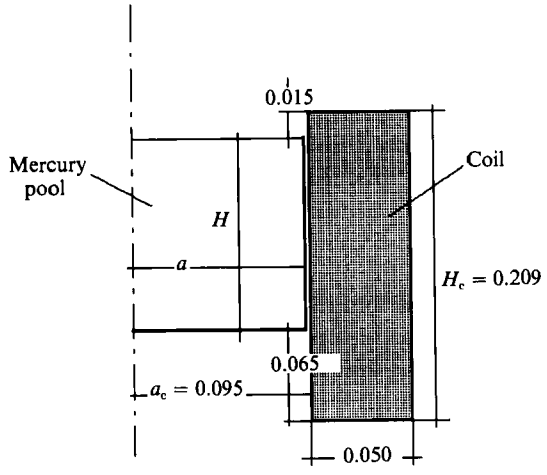

FIGURE 1. Diagram of the apparatus. Dimensions in m.

involves a kind of Froude number F whose experimental value is $\leqslant 1$. These estimates will be used in the discussion of §5.

In our experiments, although the value of N does not exceed 0.1, both phenomena are still observable and often strongly coupled. Therefore, in order to separate each phenomenon, bulk flow and free-surface motion observations have been made in different frequency ranges. For the bulk flow, the operating frequency is not less than 14 Hz to avoid strong free-surface deformations. On the other hand, to minimize the mean part of the electromagnetic forces, hence the mean motion, free-surface measurements are performed in the frequency range from 2 to 10 Hz at most.

The experimental apparatus and the measurement instrumentation are described in §2. Characterization of the bulk flow is achieved in §3. Section 4 presents investigations of the free-surface motion. The experimental results are discussed in §5 and compared with theoretical estimates.

2. Apparatus and instrumentation

The experimental ladle consists of a stainless-steel cylindrical tank filled with mercury and surrounded by a 360-turn induction coil (see figure 1). Bulk velocity measurements are made in a pool whose radius and height respectively are $a = 89$ mm and $H = 113$ mm. As for the free-surface motion characterization the dimensions of the pool are $a = 94$ mm and $H = 124$ mm. The tank is cooled by maintaining a thin film of cold water over the outside wall, and the bath temperature does not exceed 35 °C. The inductor is supplied with single-phase electrical currents with various frequencies in the range 2–22 Hz. For the electrical current source the ratio between the amplitude of the harmonics and that of the fundamental frequency does not exceed 10^{-4}. The corresponding shield parameter can be varied from 0.15 to 1.48. Mean and turbulent velocity measurements are achieved by means of hot-film probes supplied by a constant-temperature anemometer (TSI IFA 100). Such a probe is not really directional. That drawback may be avoided by only performing velocity measurements in regions where the direction of the mean velocity is known *a priori*. The procedure and a discussion of the validity of the results is detailed in Taberlet & Fautrelle (1985). We simply remind the reader that the error in the velocity measurements is approximately 20%.

Frequency f (Hz)	Shield parameter R_ω	Coil intensity I (A)	Alfvén speed u_A (m/s)
14	0.93	150	1.790
18	1.20	120	1.434
22	1.48	98	1.170

TABLE 1. Standard operating conditions for the bulk flow investigations

Concerning the bulk flow investigations, the velocities are normalized by the Alfvén speed. The typical magnetic field value B_0 used to calculate u_A is related to the coil current I by Nagaoka's empirical formula:

$$B_0 = \mu N_c I/(H_c(1+0.88\,a_c/H_c)),$$

where H_c, a_c, N_c respectively denote the height, the internal radius and the number of turns of the coil. The dimensions of the coil are detailed in figure 1. The standard operating conditions are summarized in table 1 below.

For the free-surface deformations, the amplitudes were measured by means of an electric pin. The accuracy on the height of the free surface is of the order of 0.5 mm. We have managed to minimize the mechanical vibrations induced by the coil on the tank and the probes. We have also checked that direct induction of electrical currents in the probe was negligible.

3. Bulk motion

Bulk velocity measurements have been achieved for $f = 14$, 18 and 22 Hz. We have not explored frequencies less than 10 Hz. Indeed, as we shall see later, the amplitude of the free-surface motions becomes no longer negligible when $f \leqslant 10$ Hz.

The bulk flow has many similarities with that observed by previous authors (Moore & Hunt 1984; Trakas *et al.* 1984; Taberlet & Fautrelle 1985). Its main characteristics can be summarized as follows: (i) the flow pattern is independent of the magnitude of the magnetic field in the turbulent regime; (ii) the mean and turbulent velocities are proportional to the magnetic field strength.

We shall not give details on the above well-known characteristics. We shall, rather, focus on the new features arising in this regime.

3.1. *The mean flow*

The structure of the mean flow is very similar to that observed in the previous investigations already quoted. It consists of two axisymmetric counter-rotating vortices as shown in figure 2. The flow configuration is not sensitive to variations of the frequency in the range considered here, and the radial velocity profiles across the eye of a vortex do not exhibit significant changes (cf. figure 3). Figure 4 shows the evolution of the characteristic velocity u_0, obtained by averaging the modulus of the mean velocity along the axis of the pool, with respect to the frequency. The amplitude of the characteristic velocity decreases rapidly as the frequency decreases. It is noticeable that the decay is much more rapid than the theoretical law:

$$u_0 \propto R_\omega$$

deduced from simple orders of magnitude (Taberlet & Fautrelle 1985) and from the numerical computation of the turbulent flow presented in Appendix A.

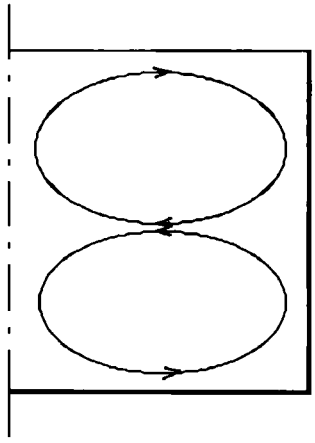

FIGURE 2. Structure of the observed mean flow pattern for all frequencies.

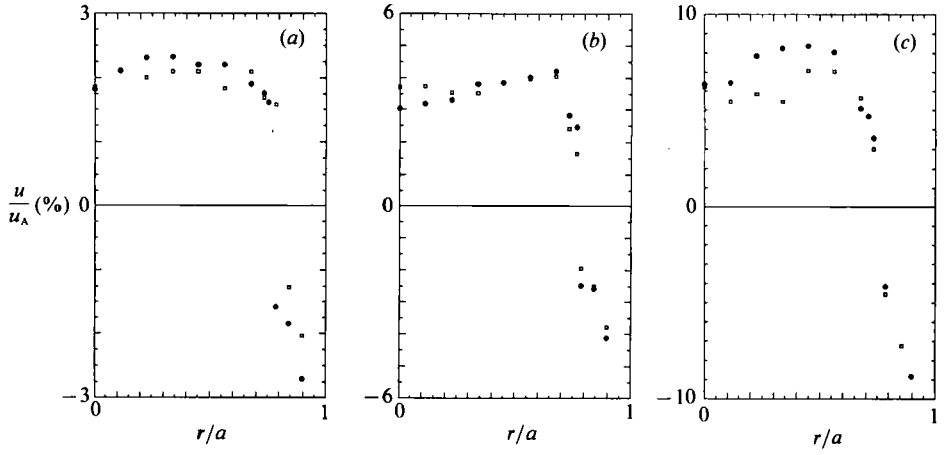

FIGURE 3. Mean radial velocity profile across the eyes of the vortices (□, upper vortex; ●, lower vortex): (a) $R_\omega = 0.93\,(z/H = 0.19, 0.76)$; (b) $R_\omega = 1.20\,(z/H = 0.23, 0.72)$; (c) $R_\omega = 1.48\,(z/H = 0.23, 0.72)$.

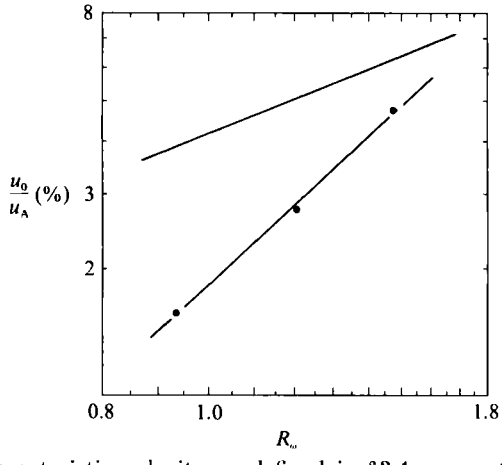

FIGURE 4. Mean characteristic velocity u_0 defined in §3.1 versus the shield parameter R_ω (the velocities are normalized by the Alfvén speed u_A): ●, experimental values; numerical computations using a standard k–ϵ model (cf. Appendix A).

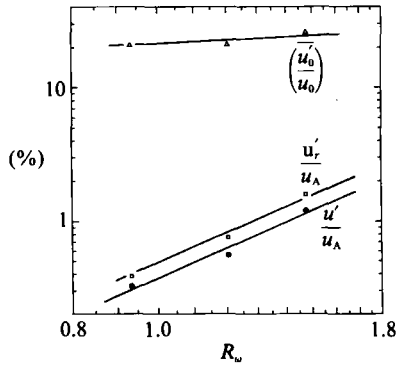

FIGURE 5. Evolution of the turbulent fluctuations with respect to the shield parameter R_ω: ●, fluctuating axial velocity component (r.m.s.) averaged along the radius through the core of the lower vortex and normalized by the Alfvén speed; □, fluctuating axial velocity component averaged along the axis of the pool; △, turbulent intensity on the axis of the pool.

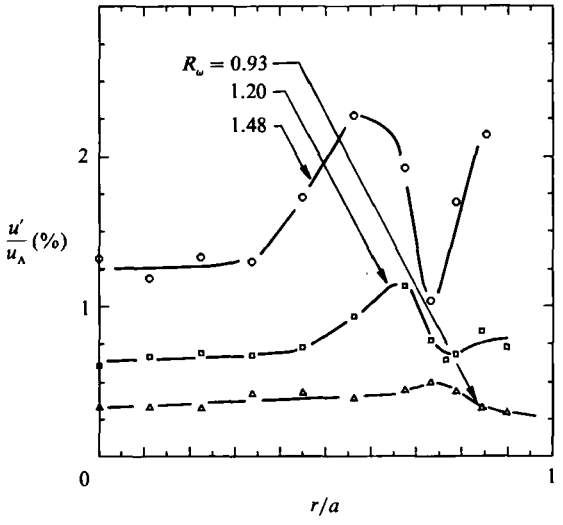

FIGURE 6. Radial profiles of the fluctuating axial velocity component through the eye of the lower vortex for various frequencies (the velocity is normalized by the Alfvén speed u_A): △, $R_\omega = 0.93$, $z/H = 0.76$; □, $R_\omega = 1.20$, $z/H = 0.72$; ○, $R_\omega = 1.48$, $z/H = 0.72$.

3.2. *Overall features of the turbulence*

The overall features of the turbulence in that configuration are not much different from those observed in the previous investigations. Let us first consider the distribution of the fluctuating velocity u'. Turbulence intensity remains high as shown in figure 5 and slowly increases with the frequency. Moreover, the fluctuating velocities vary linearly with the magnetic field. Regarding their spatial distribution, the radial profiles become flatter and flatter as the frequency decreases (cf. figure 6).

Turbulent energy spectra are shown in figure 7 (*a–c*). Note that these spectra do not exactly correspond to monodimensional turbulent ones, because of the quite high values of the turbulence intensity. Frequency spectra are converted into wavenumber spectra by means of the Taylor hypothesis. They are similar to those encountered in usual turbulent shear flows. It is interesting to observe that the integral scales are of

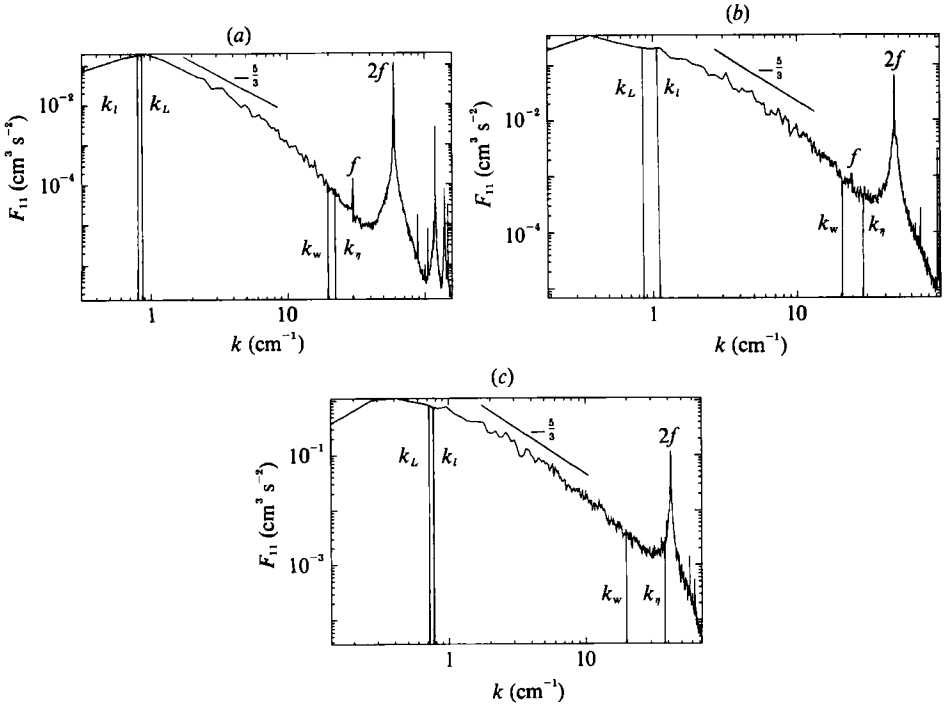

FIGURE 7. One-dimensional wavenumber spectra for various frequencies (L, l_w, η respectively denote the integral scale, the probe-sensor length, the Kolmogorov scale; $l = u'^3/\epsilon$; the length scales are converted into wavenumbers): (*a*) $R_\omega = 0.93$, $r = 0$, $z/H = 0.76$, $I = 150$ A, mean velocity $U = 2.9$ cm/s; (*b*) $R_\omega = 1.20$, $r = 0$, $z/H = 0.23$, $I = 120$, A, mean velocity $U = 4.9$ cm/s; (*c*) $R_\omega = 1.48$, $r = 0$, $z/H = 0.23$, $I = 98$ A, mean velocity $U = 6.7$ cm/s.

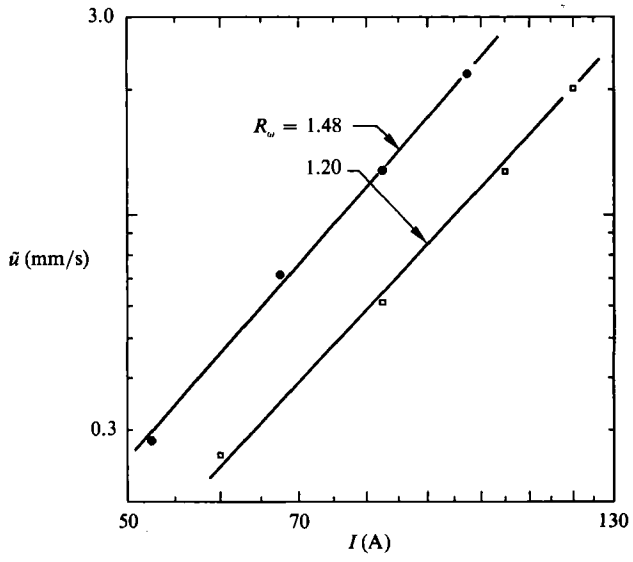

FIGURE 8. Evolution of the oscillating velocity $\tilde{u}$ with respect to the coil current for a fixed frequency in the eye of the upper vortex: □, $R_\omega = 1.20$; ●, $R_\omega = 1.48$.

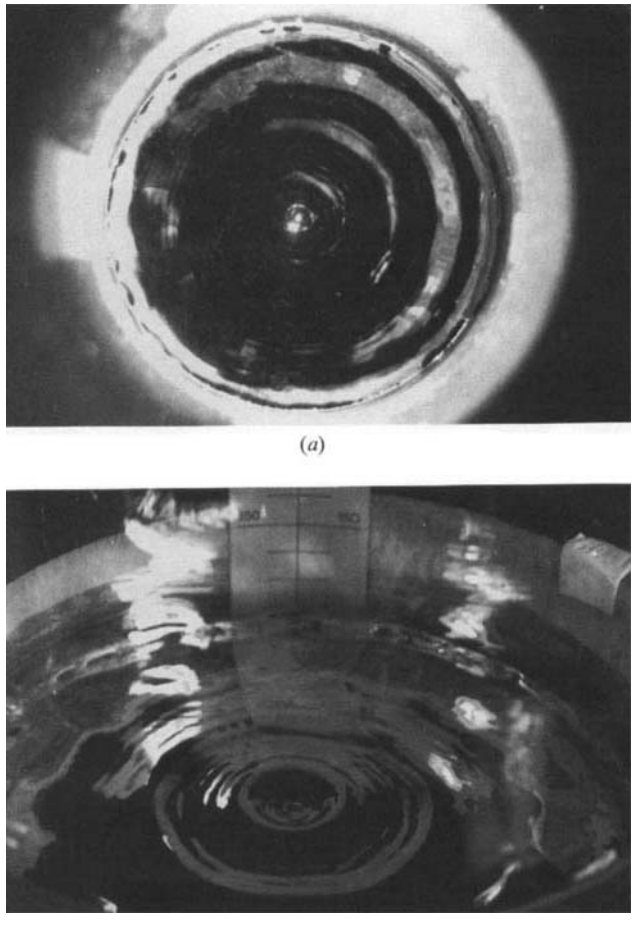

(*a*)

(*b*)

FIGURE 9. View of the free surface near the transition between the type I and type II regimes ($f = 4.2$ Hz, $I = 45$ A): (*a*) top view, (*b*) side view.

order of 6 cm, which is physically consistent with the size of the vessel. The energy spectra exhibit a main peak for a wavenumber corresponding to the frequency $2f$. The amplitude of these peaks increases as the frequency of the applied electrical currents decreases. The frequency of the dissipation scales as well as the frequency corresponding to the probe size are smaller than $2f$. It is however believed that the various peaks correspond to liquid motions (it has been checked that probe vibrations were negligible). For $f = 14$ Hz the harmonic and subharmonic frequencies are clearly apparent.

3.3. *Oscillating velocities*

Attention was focused on the oscillating part of the velocity $\tilde{u}$ corresponding to the frequency $2f$. The oscillating velocity was extracted from turbulence spectra by integrating the spectral energy density in the vicinity of the peak $2f$.

It should be emphasized that the value of $\tilde{u}$ might be underestimated. Indeed, figure 7 (*a–c*) shows that the wavenumber corresponding to the probe size (l_w) is much smaller than that corresponding to the peak of the oscillating velocity. A significant attenuation of the peak amplitude may be expected, the filtering effect increasing as

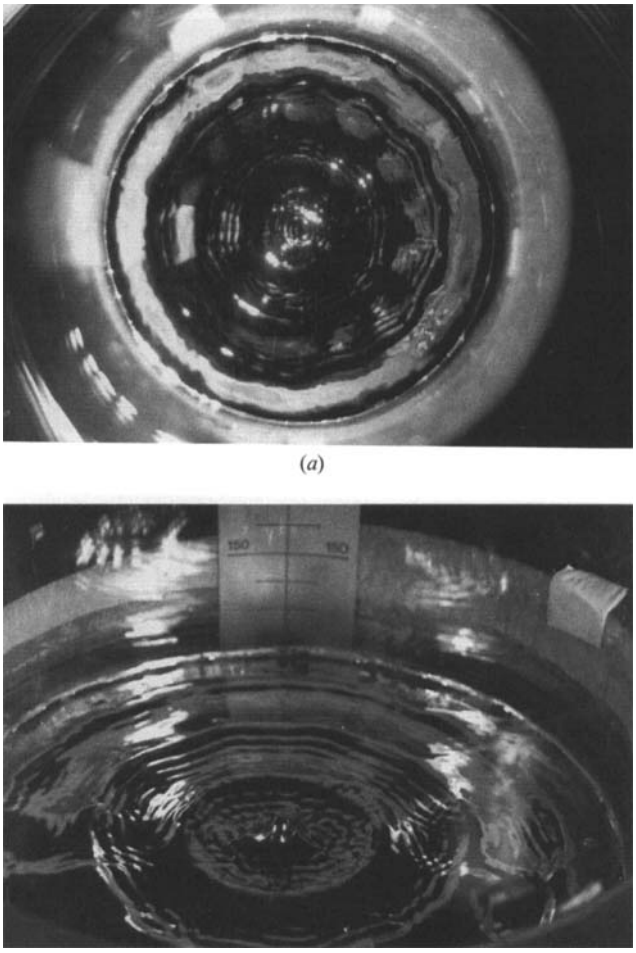

(a)

(b)

FIGURE 10. View of the free surface in the type II regime ($f = 4.2$ Hz, $I = 75$ A); (a) top view, (b) side view.

the frequency decreases. Therefore, the results concerning the oscillating velocities should only be considered as orders of magnitude.

We observe from the turbulence spectra and the oscillating velocity profiles that the oscillating velocities represent an important contribution to the fluctuations. For the lowest frequency, i.e. $R_\omega = 0.93$, the average ratio $\tilde{u}/u'$ is of the order of 40%.

As for the influence of the magnetic field strength (figure 8), the amplitude of the oscillating velocity increases very rapidly. In the range considered here, it varies roughly like I^m with $m \approx 3$.

4. Free-surface motions

The existence of an oscillating electromagnetic force leads to free-surface oscillations which consist of standing waves. Various complex phenomena occur depending on the values of both the magnetic field strength or coil current I and its frequency f. Note that, even for low frequencies ($f < 10$ Hz) the bulk motion is still

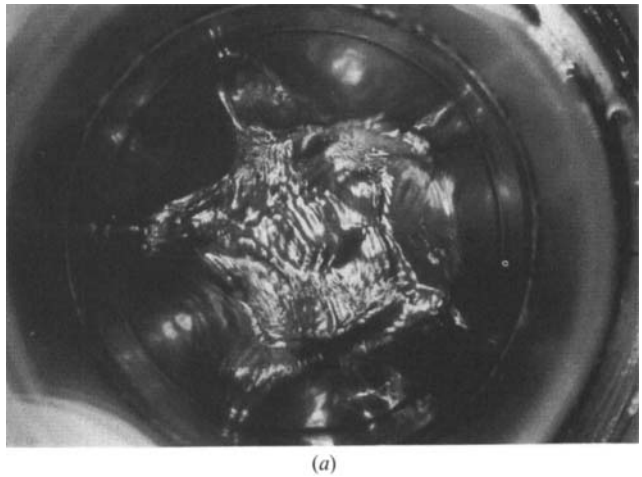

(*a*)

(*b*)

FIGURE 11. View of the free surface in the type III regime ($f = 4.2$ Hz, $I = 110$ A): (*a*) top view, (*b*) side view.

non-zero and slightly influences the free-surface motion. Extrapolation of the experimental data of figure 4 yields an estimate of the mean velocity magnitude at the lowest frequencies. For $f = 4$ Hz and $I = 120$ A for example, the mean velocity is of order 1 mm/s. Therefore, we shall not present here an exhaustive study of the phenomenon but rather try to point out some important features.

Before detailing the observations, it is useful to explain qualitatively the main features of the phenomenon. The free-surface motions may be split into two kinds of standing waves: (i) concentric standing waves which are directly forced by the alternating part of the Lorentz forces; (ii) azimuthal waves whose origin is assumed to be the instability of the previous system.

In the present cylindrical geometry, η may be expanded in Fourier–Bessel series of the modes (n, m) as follows:

$$\eta = a \sum_{m=0}^{\infty} \sum_{n=1}^{\infty} \hat{\eta}(t)\, S_{nm}(r) + \text{c.c.},$$

(a)

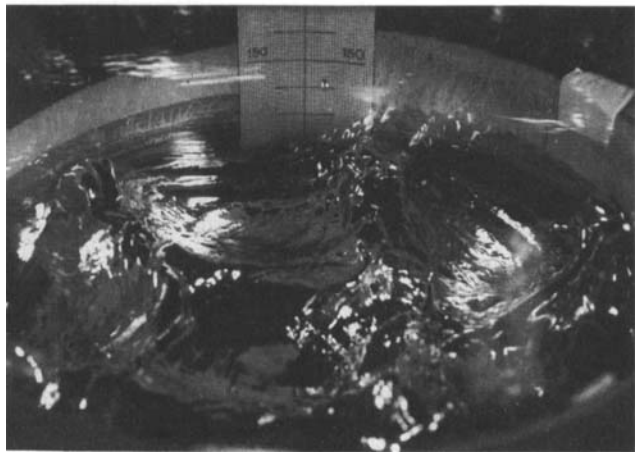

(b)

FIGURE 12. View of the free surface in the type IV regime ($f = 4.2$ Hz, $I = 180$ A): (a) top view, (b) side view.

with $S_{nm} = \exp(im\theta) J_m(\lambda_n r)$, where J_m is a Bessel function of order m of the first kind, and $\lambda_n a$ the nth zero of $J'_m(\lambda_n a)$. The surface waves will be represented by the couple (n, m), where n and m are integers corresponding to the above Fourier–Bessel decomposition of the free-surface deformation.

4.1. *The various surface patterns*

The free surface exhibits various wave configurations according to the values of I and f. In the (I,f)-plane, we have qualitatively observed four regions corresponding to four types of regime. Note that the boundary between the various regimes was not easy to observe precisely especially for low and high frequencies because of the complexity of the transitions. For fixed frequencies and increasing values of the magnetic field, figures 9–16 illustrate the various regimes for two typical frequencies, namely $f = 4.2$ and 10.3 Hz. The transition diagram is shown in figure 17. The characteristics of the observed dominant modes corresponding to the points of the regime boundaries are collected in table 2. Their main features are the following:

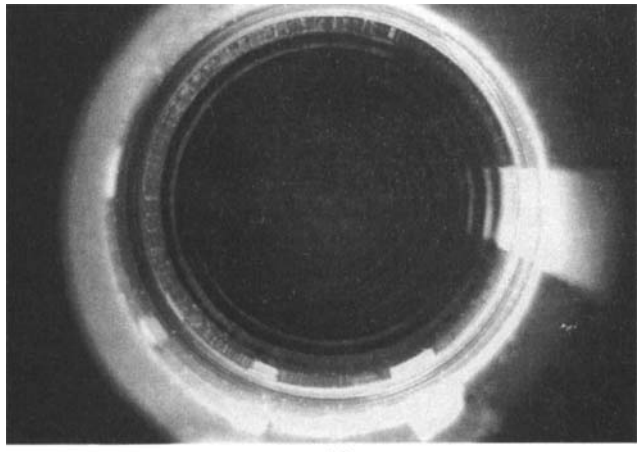

(*a*)

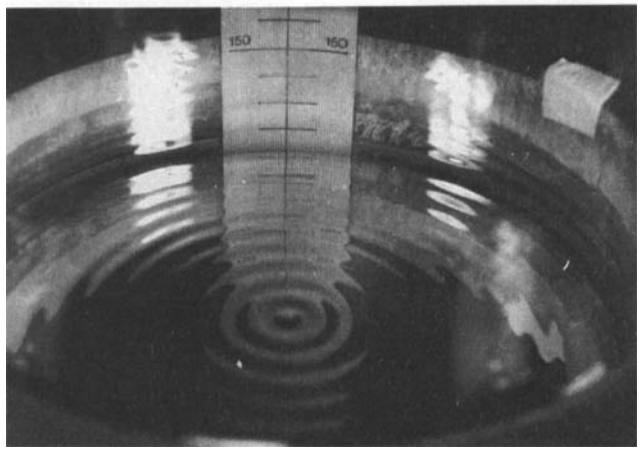

(*b*)

FIGURE 13. View of the free surface near the transition between the type I and type II regimes ($f = 10.3$ Hz, $I = 30.2$ A): (*a*) top view, (*b*) side view.

(i) *Type I regime*: the free-surface motion consists of axisymmetric standing waves whose dominant frequency is $2f$;

(ii) *Type II regime*: it is characterized by the appearance of azimuthal waves superimposed on concentric waves; the dominant frequency of both concentric and azimuthal waves is still $2f$;

(iii) *Type III regime*: large-amplitude and low-wavenumber azimuthal waves are set up after a subharmonic transition; the modes (n, m) of those waves are selected by the applied frequency, and the concentric waves are no longer observable;

(iv) *Type IV regime:* the free-surface deformation becomes strongly chaotic.

We have observed that the transitions occurred with hysteresis. The experimental evidence of the existence of a type II regime is not always clear (e.g. for $f = 10.3$ Hz). Furthermore, the type II wave amplitudes are generally small, and the precise determination of the dominant mode is quite difficult and is possible only in the low-frequency range. It may be noticed that the eigenfrequency of the type II azimuthal waves is close to $2f$ (the eigenfrequencies of the first surface free modes are given in

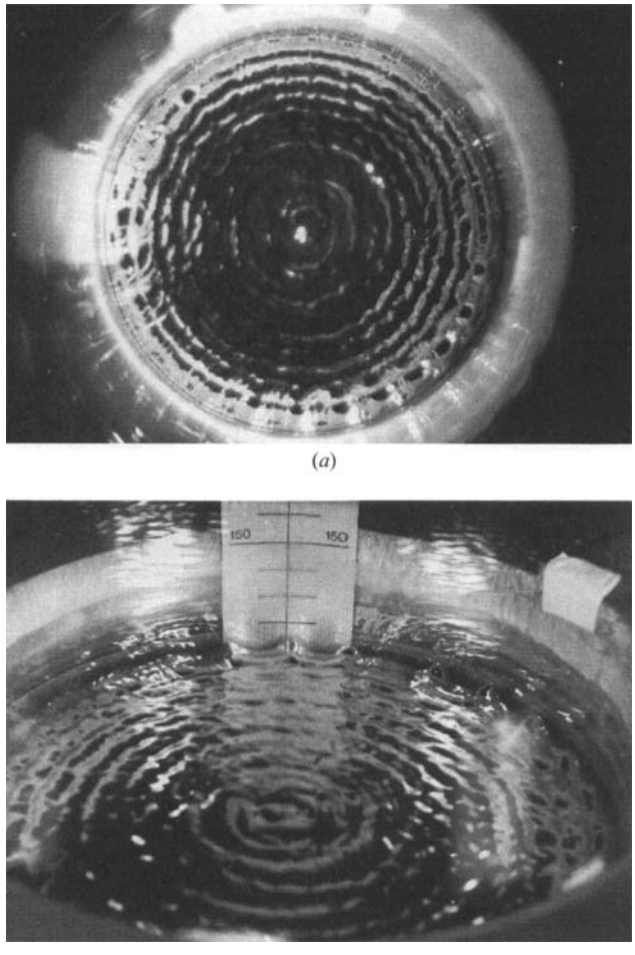

(a)

(b)

FIGURE 14. View of the free surface near the transition between the type II and type III regimes ($f = 10.3$ Hz, $I = 75$ A): (a) top view, (b) side view.

table 3 of Appendix B). The transitions between the various regimes are not clearcut. It seems that for the same coil current there may coexist on the free surface several patterns. For example, in figures 9 and 13, a slight symmetry breaking of the concentric regime appears (at the edge of the pool in figure 13). In figure 14, the wave pattern is a superposition of a type II and a type III regime. It is observed that the type III waves exhibit in that case both a temporal and a spatial modulation.

In the type IV regime an interesting feature is the appearance of strong intermittent small-scale jets which eject liquid metal from the bath. These bursts are observable in figure 16(b).

4.2. *Influence of the coil intensity*

For a fixed magnetic field frequency, it is of interest to determine the influence of the coil intensity on the amplitude of the waves. The measurements have been made at the centre and the side of the tank to separate respectively concentric modes from azimuthal ones. Figure 18(a–c) shows the evolution of the amplitudes of the two

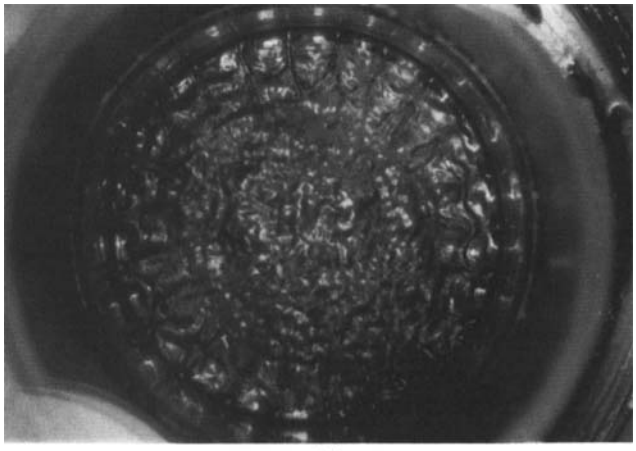

(*a*)

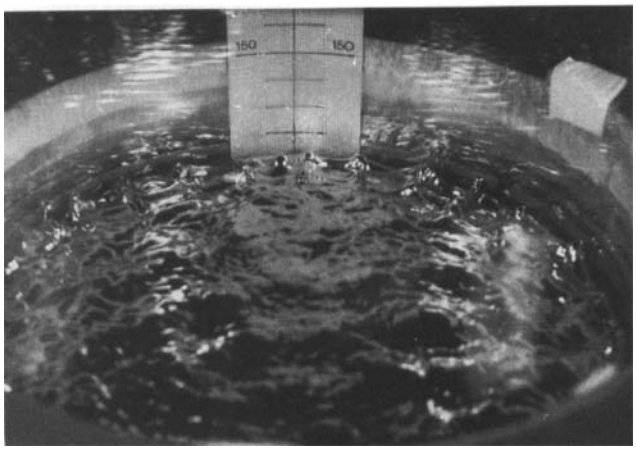

(*b*)

FIGURE 15. View of the free surface in the type III regime ($f = 10.3$ Hz, $I = 140$ A): (*a*) top view, (*b*) side view.

kinds of waves with respect to the coil current for $f = 2.03$, 4.05 and 7.02 Hz. The growth depends on the frequency as well as on the nature of the wave regime.

At a pool centre, the amplitude is a growing function of the coil intensity. In the type I regime, the amplitude grows approximately like I^{α} with α varying from 1.6 to 2.4 according to the frequency of the inductor current. The value $\alpha = 2.4$ has been observed for the lowest frequency $f = 2.03$ Hz. Figure 18(*b*) shows one of the few cases where we have been able to observe the amplitude evolution of the concentric modes in the type II and type III regimes. The amplitude exhibits a reduction in growth after the transition between the type I and the Type II regime and varies approximately as $I^{0.8}$ in the type II regime.

The behaviour of the amplitude of the azimuthal waves has been investigated by making measurements at the pool side. Figure 18(*c*) shows first a sharp growth of their amplitude near the transition between the type II and the type III regimes. Then, the amplitude grows like $I^{1.6}$. That evolution is very different from that of the concentric modes.

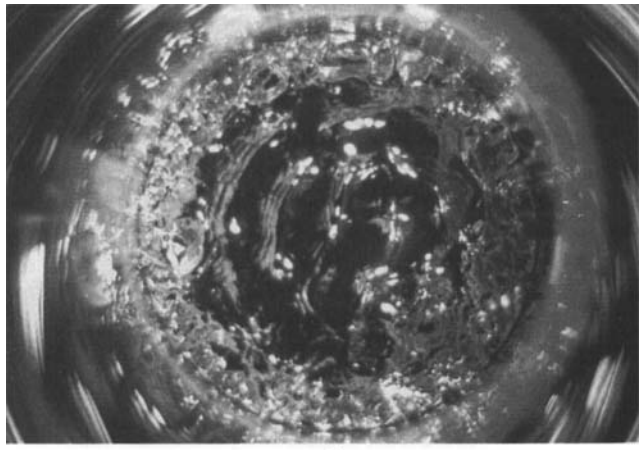

(*a*)

(*b*)

FIGURE 16. View of the free surface in the type IV regime ($f = 10.3$ Hz, $I = 210$ A); (*a*) top view, (*b*) side view.

4.3. *Influence of the frequency*

Analogous amplitude measurements have been performed for a fixed coil intensity and varying frequencies. Two cases have been explored, namely $I = 90$ and 150 A corresponding respectively to type III and type IV regimes. The evolution presented in figures 19–21 is somewhat complex especially for frequencies less than 4 Hz, although this is not obvious owing to the use of the logarithmic scales. This is consistent with the complexity of the stability diagram of figure 17. The scatter of the experimental data (e.g. in figure 19) comes from the fact that the wave pattern also changes with the frequency. Globally, the amplitudes are decreasing as the frequency increases and become negligible when $f \geqslant 10$ Hz. The decay law also depends on the coil intensity. The amplitudes of the waves at the pool side behave like f^{-3} and $f^{-1.8}$ for $I = 90$ and 150 A respectively. The azimuthal wavelengths are also decreasing functions of the frequency. This seems to be a simple consequence of the fact that the dominant mode is of higher order as the frequency increases, as shown in table 2.

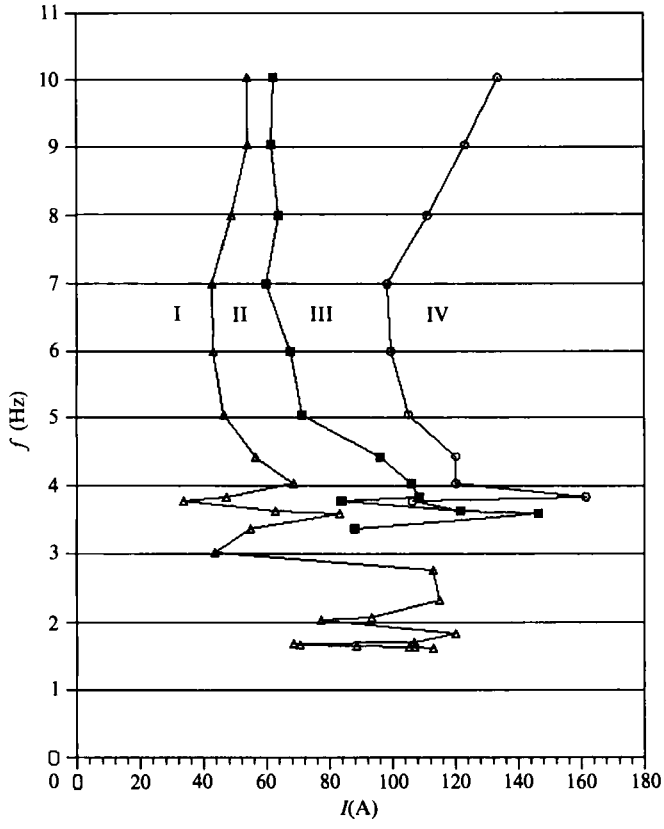

FIGURE 17. Stability diagram in the (I,f)-plane showing the various flow regimes: △, type I–type II transition; ■, type II–type III transition; ○, type III–type IV transition.

4.4. *Energy spectra*

A hot-film probe has been used to investigate the spectral content of the surface waves by recording liquid velocity fluctuations. The velocity probe was located under the free surface at the pool centre and at the pool side. Figures 22–24 show the spectra corresponding to the various regimes for $f = 4.05$ Hz.

For the type I regime, the spectrum of figure 22 exhibits sharp peaks, and the background noise remains very weak. The dominant frequency is $2f$, although the subharmonics frequency f and its harmonics (e.g. $3f$) are non-negligible. In the type II regime of figure 23, the dominant frequency is still $2f$. However, it must be observed that: (i) the $2f$ peak is broader than that of the previous case; (ii) a continuous part appears in the very low-frequency region of the spectrum. The presence of a bulk motion cannot fully explain the origin of that phenomenon. The extrapolated bulk velocity amplitude (≈ 0.6 mm/s) seems too weak to be consistent with the quite high level of the continuous part which correspond to a typical velocity of 5 mm/s. It is believed that the widening of the spectra comes from the wave motion itself. In the type III regime (figure 24) the subharmonic frequency emerges as the dominant one.

Frequency (Hz)	Type I regime	Type II regime	Type III regime
1.625	(1,0)	(0,3)+(1,0)	—
1.627	(1,0)	(0,3)+(1,0)	—
1.635	(1,0)	(0,3)+(1,0)	—
1.649	(1,0)	(0,3)+(1,0)	—
1.667	(1,0)	(0,3)+(1,0)	—
1.684	—	—	—
1.700	—	—	—
1.834	(2,0)	(1,4)+(2,0)	—
2.046	(3,0)	(1,5)+(3,0)	—
2.082	—	—	—
2.336	(4,0)	(1,7)+(4,0)	—
2.773	(6,0)	(1,10)+(6,0)	—
3.025	—	—	—
3.367	(6,0)	(1,14)+(6,0)	(1,3)
3.591	(6,0)	(1,15)+(6,0)	(1,4)
3.636	—	—	(1,4)
3.770	—	—	(1,4)
4.030	(8,0)	—	(1,5)
4.428	(9,0)	—	(1,6)
5.051	—	—	(1,8)
5.998	(12,0)	—	(1,12)
6.997	(14,0)	—	(1,16)
7.995	—	—	(1,19)
9.029	—	—	(1,22)
10.029	(22,0)	—	(1,24)

TABLE 2. Values of the observed dominant modes (no indication means that it was not possible to determine the characteristics of the mode)

5. Discussion

The observed bulk flow has many similarities to the electromagnetically driven flows studied in single-phase configurations. For the present case, the main peculiarities are: (i) the presence of an alternating velocity which is superimposed on turbulent fluctuations; (ii) the rapid decay of the characteristic mean velocity with respect to the frequency.

It is of interest to compare the characteristic mean velocities by a standard k–ϵ model (cf. Appendix A) and the experimental ones. The evolution of the computed velocity in figure 4 is consistent with the asymptotic behaviour of the electromagnetic forces in (A 5). However, it is observed from figure 4 that the experimental decay is much more rapid than the theoretical one, which does not take into account the effect of the alternating electromagnetic force. The physical mechanism that leads to a faster decay of the mean velocity, is not well understood. This phenomenon could possibly be attributed to either (i) the effect of the electric currents induced by the $(\boldsymbol{u} \times \boldsymbol{B})$ term which has been neglected in the computation; or (ii) the additional dissipation due to the presence of alternating velocities.

As for the first explanation, the $\boldsymbol{u} \times \boldsymbol{B}$ term has been shown to reduce the efficiency of the mean motion (Glière, Fautrelle & Masse 1988) when the ratio $u_0/a\omega$ is of order of unity. But, in the present case, the maximum value of that non-dimensional parameter is approximately 0.22. Thus, the electrical currents induced by the fluid motion across the magnetic lines of force remain small compared with the so-called

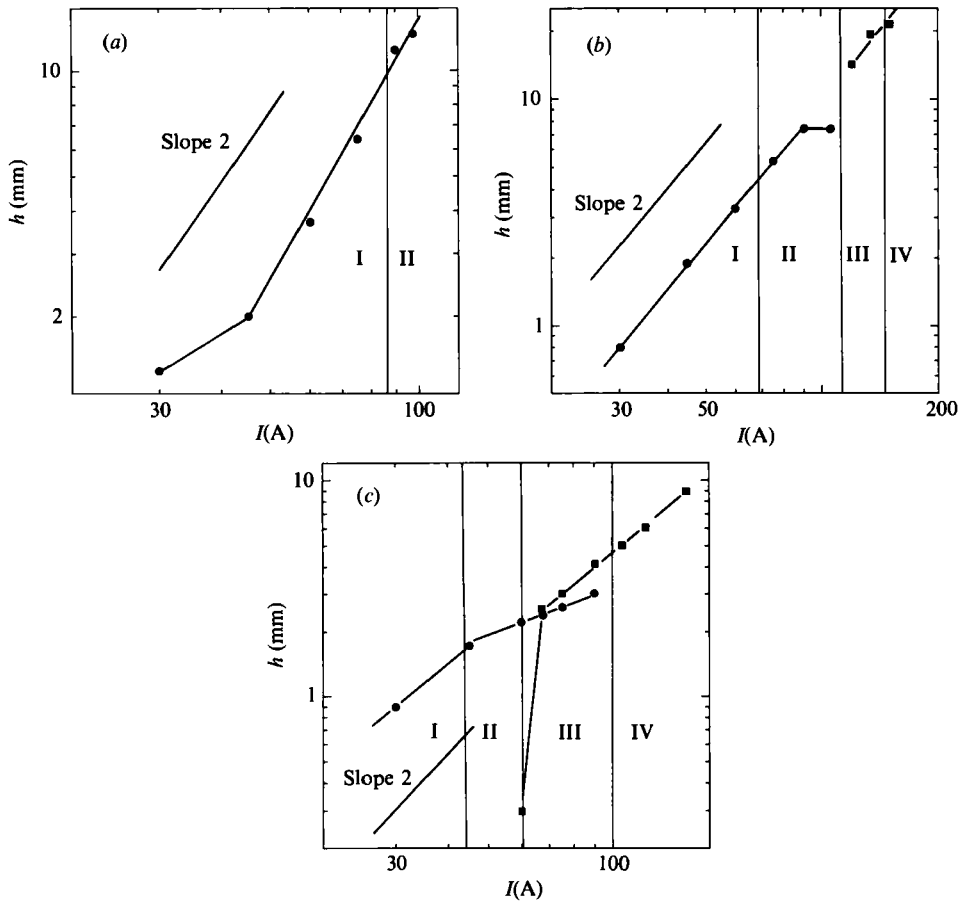

FIGURE 18. Evolution of the surface wave amplitude with respect to the coil current at the centre (●) and the side of the pool (■): (*a*) $f = 2.03$ Hz, (*b*) $f = 4.05$ Hz, (*c*) $f = 7.02$ Hz.

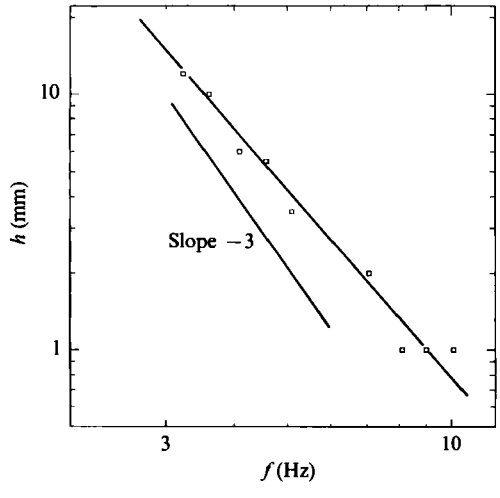

FIGURE 19. Evolution of the amplitude of the surface waves at the pool centre with respect to the frequency for $I = 90$ A.

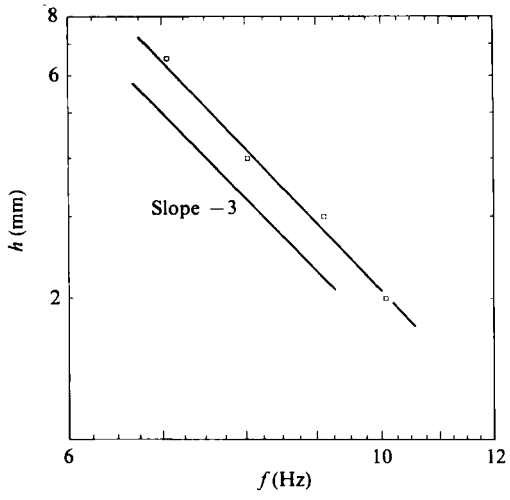

FIGURE 20. Evolution of the amplitude of the surface waves at the pool side with respect to the frequency for $I = 90$ A.

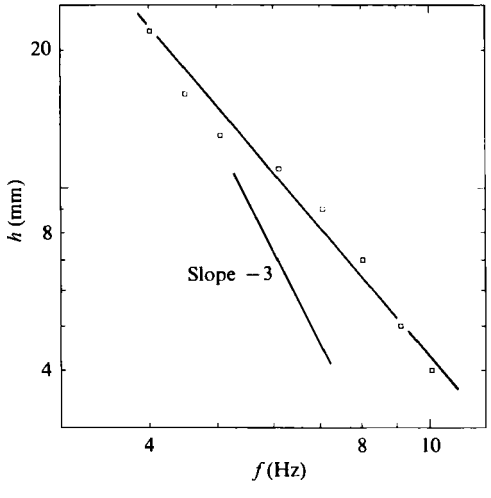

FIGURE 21. Evolution of the amplitude of the surface waves at the pool side with respect to the frequency for $I = 150$ A.

'eddy currents'. As for the existence of an additional dissipation, no clear mechanism has been found. Furthermore, the measurements of the turbulent dissipation rates do not show any noticeable growth as R_ω is decreasing. We recall, however, that the accuracy of the measurements of ϵ is possibly rather weak.

The free-surface motion observed here has revealed complex phenomena, and the present investigations are only preliminary observations. The present phenomena have some similarities with other related problems. The oldest one is the so-called Faraday problem which deals with the excitation of the free surface of a liquid in an oscillating tank (Faraday 1831; Benjamin & Ursell 1954; Ciliberto & Gollub 1985). Alternating electric fields have also been shown to generate free-surface waves (Briskman & Shaidurov 1968). The present case seems to be more complicated than the previous one in the sense that various types of transition occur. Schematically, the configurations may be split into two different kinds of wave systems (cf. §4).

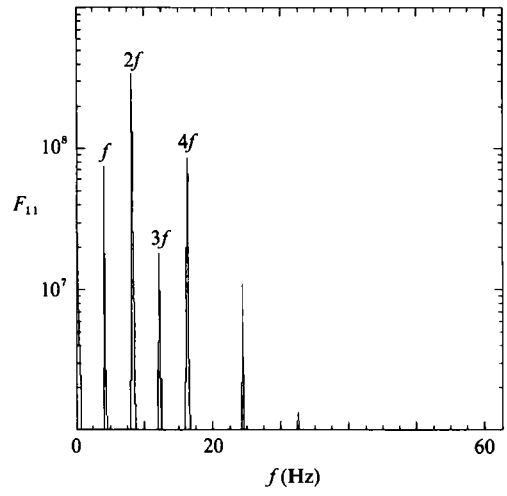

FIGURE 22. One-dimensional energy spectrum of the oscillating motion under the free surface in the type I regime for $f = 4.05$ Hz and $I = 27$ A at the pool centre (the vertical units are arbitrary).

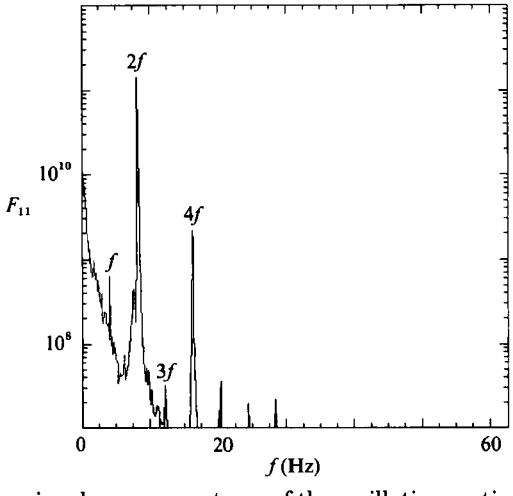

FIGURE 23. One-dimensional energy spectrum of the oscillating motion under the free surface in the type II regime for $f = 4.05$ Hz and $I = 85$ A at the pool side (the vertical units are arbitrary).

The first wave system consists of axisymmetric waves whose dominant oscillation frequency is $2f$. This is shown by the spectra of figures 22 and 23. Concentric waves first appear for low magnetic field values. According to GFS, the axisymmetric wave system is directly forced by the oscillating part of the Lorentz forces. This is also confirmed by the fact that the eigenfrequency of the observed dominant mode is equal to the Lorentz force frequency. When the amplitude of the forced concentric waves becomes sufficiently large, nonlinear effects may explain some observations, namely: (i) the subharmonic frequency revealed by free-surface measurements at the pool centre and superimposed to the dominant one; (ii) the appearance of transversal waves in the type II regime due to the possible instability of the concentric modes (see for example Craik 1985; Miles & Henderson 1990).

GFS have studied theoretically the stability of the free surface of a liquid metal under the influence of parallel alternating electric currents. They have shown that

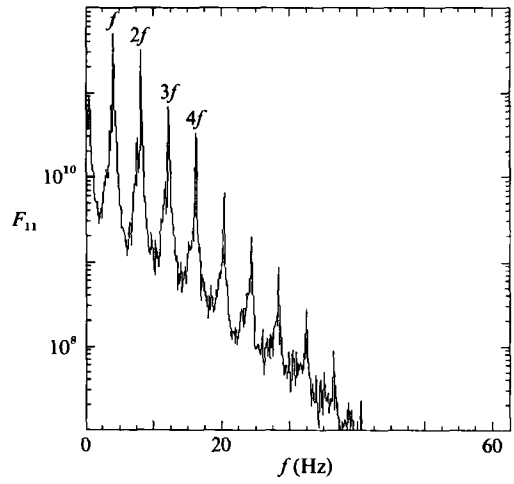

FIGURE 24. One-dimensional energy spectrum of the oscillating motion under the free surface in the type III regime for $f = 4.05$ Hz and $I = 165$ A, at the pool side (the vertical units are arbitrary).

any azimuthal free-surface perturbation leads to perturbations of the electromagnetic forces which reinforce the free-surface deformation. It is not possible to make a precise comparison between the theoretical results and our experiments. In the situation considered by GFS, the investigations concern only a linear stability analysis. Nevertheless, they have shown that the growth of non-axisymmetric modes is governed by a coupled system of Mathieu equations. The most easily excited transition to non-axisymmetric modes occurs for modes whose eigenfrequency f_0 is close to nf, with $n = 1, 2, \ldots$. For $n = 1$, the transition corresponds to the main primary (strong) resonance. For $n > 2$, secondary (weak) resonance occur.

It was not easy to determine the dominant mode of the type II waves because of their generally small amplitude. However, in the cases where it was possible to identify the wave pattern without ambiguity it is shown that the eigenfrequency f_0 of the observed type II dominant mode is close to the frequency of the electromagnetic forces ($2f$). Thus, their origin might also be due to secondary parametric resonance which occur when f_0 is close to $2f$ (i.e. $n = 2$ in GFS). Those resonances are weak, and that is consistent with the small amplitudes observed in that type of transition.

The third wave system consists of subharmonic azimuthal waves. That system occurs for sufficiently large magnetic field values. The transition is characterized by a very sharp increase of the amplitude of the waves. The resulting amplitude is generally much larger than that corresponding to the previous system. This subcritical-type behaviour is consistent with the hysteresis observed in the transitions. The eigenfrequency f_0 of the dominant mode is shown to be close to f (i.e. $n = 1$ in GFS), corresponding to primary parametric resonances.

It is of interest to compare the experimental evolution laws of the amplitude of the waves to the theoretical estimates (5), (6). For a fixed frequency, from a simple balance between gravity, inertia and the electromagnetic forces it might be theoretically expected that the wave amplitudes exhibit: (i) a quadratic variation with respect to the coil intensity in the small-amplitude regime; (ii) a linear variation in the large-amplitude regime. Such tendencies do not contradict the experimental results. However, discrepancies have been observed (see for example figure 18*a–c*), indicating that more complex phenomena occur. Here too, the concentric and

azimuthal wave systems do not have the same behaviour. For example, in figure 18(*b*) the growth laws of the concentric and azimuthal system are very different in the type II and III regimes.

Similar conclusions have been drawn from the comparison between the experimental and theoretical amplitude evolutions for a fixed coil intensity and varying frequencies. For intermediate coil current values, the decay of the amplitude does not contradict the estimates (5), (6) which yield close decay laws, namely f^{-3} and $f^{-\frac{5}{2}}$ respectively (figures 19, 20). In that case too, we observe a slight behaviour difference between the concentric and azimuthal wave systems. However, for large coil currents, the experimental decay is very different from the simple estimate.

The present experiment has exhibited a variety of complex phenomena. The study is preliminary in the sense that only few aspects have been shown. On the one hand many questions are unanswered. On the other hand, it would be interesting to explore other cases, e.g. the bulk flow under the influence of a very low-frequency magnetic field and the intermittent free-surface ejection.

Appendix A. The electromagnetic force distribution and bulk motion

A.1. *The electromagnetic force distribution*

It is useful for the discussion to recall some characteristics of the electromagnetic forces. Let us consider a cylindrical liquid-metal pool located in a coil supplied with a single-phase alternating electric current. The geometry is supposed to be axisymmetric. The magnetic field may be calculated from an azimuthal vector potential, namely:

$$\boldsymbol{B} = \boldsymbol{\nabla}(A'\boldsymbol{i}_\theta), \tag{A 1}$$

(r, θ, z), A' denoting the cylindrical coordinates and the single component of the vector potential. The function $A'(r, z, t)$ may be split into its modulus $A(r, z)$ and its phase $\phi(r, z)$ (See for example Moreau 1980) as follows:

$$A' = A\,\mathrm{e}^{\mathrm{i}(\omega t+\phi)} + \text{c.c.} \tag{A 2}$$

The electrical current density $\boldsymbol{j}$ is obtained from the vector potential by Ohm's law:

$$j = -\sigma(\partial A'/\partial t)\, i_\theta. \tag{A 3}$$

The electromagnetic forces $\boldsymbol{j} \times \boldsymbol{B}$ may be expressed in terms of the vector potential modulus A and its phase ϕ. They entail a mean part $\langle \boldsymbol{F} \rangle$ and an oscillating one $\tilde{\boldsymbol{F}}$, namely

$$\boldsymbol{F} = \langle \boldsymbol{F} \rangle + \tilde{\boldsymbol{F}}, \quad \text{with} \quad \langle \boldsymbol{F} \rangle = -\tfrac{1}{2}\sigma\omega A^2 \boldsymbol{\nabla}\phi, \tag{A 4), (A 5}$$

$$\tilde{\boldsymbol{F}} = \tfrac{1}{2}\sigma\omega A^2 \boldsymbol{\nabla}\phi \cos(2\omega t + 2\phi) + \tfrac{1}{2}\sigma\omega \sin(2\omega t + 2\phi)\,(\boldsymbol{\nabla}(\tfrac{1}{2}A^2) + A^2 \boldsymbol{i}r/r). \tag{A 6}$$

In the low-frequency limit, the order of magnitude of A' is

$$A' = O(B_0 \lambda), \tag{A 7}$$

λ being a typical lengthscale which may be identified either with the pool radius or the free-surface motion wavelength depending on whether the bulk flow or the surface wave is considered.

Thus, the order of magnitude of the alternating electromagnetic force $\tilde{\boldsymbol{F}}$ is

$$\tilde{\boldsymbol{F}} = O(\sigma\omega\lambda B_0^2) = O(R_\omega). \tag{A 8}$$

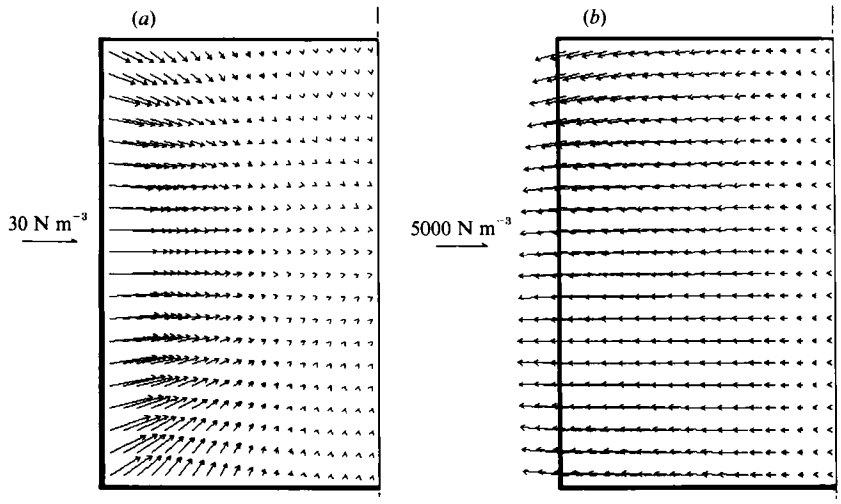

FIGURE 25. Computed distribution of the Lorentz forces in a half-meridian plane for $I = 100$ A and $f = 1$ Hz: (*a*) mean part $\langle \boldsymbol{F} \rangle$, (*b*) alternating part $\tilde{\boldsymbol{F}}$ (sine part of (A 6)).

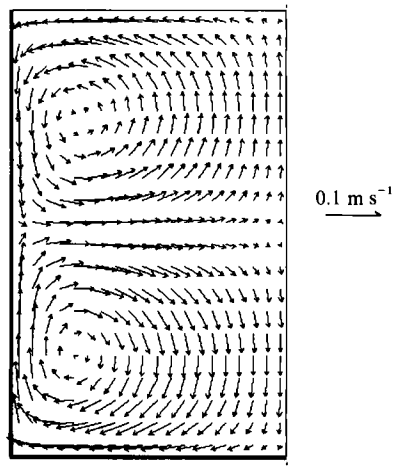

FIGURE 26. Computed mean flow pattern in a half-meridian for $I = 100$ A and $f = 14$ Hz.

As for the mean part of the Lorentz forces, the spatial phase variations are of order R_ω (Taberlet & Fautrelle 1985). Therefore, the order of magnitude of $\langle \boldsymbol{F} \rangle$ is

$$\langle \boldsymbol{F} \rangle = O(R_\omega^2). \tag{A 9}$$

Neglecting the electric current induced by the liquid motions, Maxwell equations have been solved numerically in the geometry shown in figure 1. The finite volume method, used here has been described in previous papers (see for example Barbier *et al.* 1982). Figure 25(*a*, *b*) shows the distribution of both parts of the Lorentz forces for a fixed coil current and $f = 1$ Hz. (This corresponds to $R_\omega = 0.074$.) The numerical results confirm the estimates (A 8), (A 9). Note that the spatial distributions of each part are quite different.

A.2. *Computation of the bulk motion*

It is of interest to recall the effects of the mean part of the Lorentz forces on the liquid motions. Such investigations have been done by many authors (Tarapore & Evans,

m	$n=1$	2	3	4	5
0	3.18	4.31	5.19	5.93	6.60
1	2.18	3.75	4.75	5.56	6.27
2	2.84	4.21	5.13	5.90	6.57
3	3.33	4.60	5.48	6.21	6.86
4	3.75	4.95	5.79	6.50	7.12
5	4.12	5.27	6.08	6.77	7.38
6	4.45	5.57	6.35	7.02	7.61
7	4.76	5.85	6.61	7.26	7.84
8	5.05	6.11	6.85	7.49	8.06
9	5.32	6.36	7.09	7.71	8.27
10	5.58	6.59	7.31	7.93	8.48
11	5.82	6.82	7.53	8.13	8.67
12	6.06	7.04	7.73	8.33	8.87
13	6.28	7.25	7.94	8.52	9.05
14	6.50	7.45	8.13	8.71	9.23
15	6.71	7.65	8.32	8.89	9.41
16	6.91	7.84	8.50	9.07	9.58
17	7.11	8.03	8.68	9.24	9.75
18	7.30	8.21	8.86	9.41	9.91
19	7.48	8.39	9.03	9.58	10.1
20	7.66	8.56	9.19	9.74	10.2
21	7.84	8.73	9.36	9.90	10.4
22	8.01	8.89	9.52	10.1	10.5
23	8.18	9.05	9.67	10.2	10.7
24	8.35	9.21	9.83	10.4	10.8
25	8.51	9.37	9.98	10.5	11.0

TABLE 3. Numerical values of the natural frequencies of the vessel (in Hz)

1976; Mikelson *et al.* 1978; Moore & Hunt 1984; Barbier *et al.* 1982; El Kaddah *et al.* 1986). We have extended the previous results to the low-frequency case. The Navier–Stokes equations governing the mean velocity were solved numerically by a finite volume method (cf. Barbier *et al.* 1982). Turbulence was taken into account via an eddy viscosity calculated by means of a k–ϵ model.

Figure 26 illustrates the flow pattern for $f = 14$ Hz and $I = 100$ A. It consists of two counter-rotating vortices, in agreement with the experiments of §3. It is of interest to consider the evolution of the computed characteristic velocity u_0 with respect to the shield parameter R_ω in the low-frequency limit. In accordance with previous estimates (Taberlet & Fautrelle 1985), u_0 varies linearly with the frequency as shown in figure 4.

In summary, the computed flow pattern is consistent with the experimental one, but the velocity amplitudes are in disagreement in the frequency range considered here.

Appendix B. Eigenfrequencies of the surface free modes

The values of the eigenfrequencies of the surface free modes are given in table 3 for the present experiments.

REFERENCES

BARBIER, J. N., FAUTRELLE, Y. R., EVANS, J. W. & CREMER, P. 1982 Simulation numérique des fours chauffés par induction. *J. Méc. Théor. Appl.* **1**, 533–556.

BENJAMIN, T. B. & URSELL, F. 1954 The stability of a plane free surface of a liquid in vertical periodic motion. *Proc. R. Soc. Lond.* A **225**, 505–515.

BRISKMAN, V. A. & SHAIDUROV, G. F. 1968 Parametric instability of a fluid surface in an alternating electric field. *Sov. Phys. Dokl.* **13**, 540–542.

CILIBERTO, S. & GOLLUB, J. P. 1985 Chaotic mode competition in parametrically forced surface waves. *J. Fluid Mech.* **158**, 381–398.

CRAIK, A. D. D. 1985 *Wave Interactions and Fluid Flows*. Cambridge University Press. London.

DAHLBERG, E. 1972 On the action of a rotating magnetic field on a conducting liquid. *AB Atomenergi, Rep.* AE-447. Sweden.

DAVIDSON, P. A., HUNT, J. C. R. & MOROS, A. 1988 Turbulent recirculating flows in liquid metal MHD. Proc. 5th Beer-Sheva Seminar on MHD Flows and Turbulence. In *Liquid Metal Flow: Magnetohydrodynamics and Applications* (ed. H. Branover, M. Mond & Y. Unger). Prog. in Astron. and Aeron. vol. 111, pp. 400–420. AIAA.

EL KADDAH, N., SZEKELY, J., TABERLET, E. & FAUTRELLE, Y. R. 1986 Turbulent recirculating flow in induction furnaces: a comparison of measurements with predictions over a range of operating conditions. *Metall. Trans.* B **17**, 687–694.

FARADAY, M. 1831 On the forms and states assumed by fluids in contact with vibrating elastic surfaces. *Phil. Trans. R. Soc. Lond.* **121**, 319–340.

FAUTRELLE, Y. R. 1981 Analytical and numerical aspects of the electromagnetic stirring induced by alternating magnetic fields. *J. Fluid Mech.* **102**, 405–430.

GALPIN, J. M., FAUTRELLE, Y. R. & SNEYD, A. 1992 Parametric resonance in low-frequency magnetic stirring. *J. Fluid Mech.* **239**, 409–427 (referred to herein as GFS).

GLIÈRE, A., FAUTRELLE, Y. R. & MASSE, P. 1988 Numerical coupled model for electromagnetic stirring in continuous casting of steel. In Proc. 5th Beer-Sheva Seminar on MHD Flows and Turbulence (ed. H. Branover, M. Mond & Y. Unger) Prog. in Astron. and Aeron., vol. 111. In *Liquid Metal Flow: Magnetohydrodynamics and Applications*, pp. 481–489. AIAA.

HUNT, J. C. R. & MAXEY, M. 1980 Estimating velocities and shear stresses in turbulent flows of liquid metals driven by low frequency electromagnetic fields. In *Proc. 2nd Beer-Sheva Seminar on MHD Flows and Turbulence* (ed. H. Branover & A. Yakhot), pp. 249–269. Israel University Press.

LAMB, H. 1932 *Hydrodynamics*, 6th edn. Cambridge University Press.

MIKELSON, Y. Y., YAKOVITCH, A. T. & PAVLOV, S. I. 1978 Numerical investigation of averaged MHD-flow in cylindrical regions with the adoption of working hypotheses for turbulent stresses. *Magnit. Gidrodin.* **14**, 51–58.

MILES, J. & HENDERSON, D. 1990 Parametrically forced surface waves. *Ann. Rev. Fluid Mech.* **22**, 143–165.

MOFFATT, H. K. 1984 High frequency excitation of liquid metal systems. In *Proc. IUTAM Symp. on Metallurgical Applications of MHD, 1982, Cambridge, UK*, pp. 180–189. London: The Metals Society.

MOORE, D. J. & HUNT, J. C. R. 1984 Flow, turbulence and unsteadiness in coreless induction furnaces. In *Proc. IUTAM Symp. on Metallurgical Applications of MHD*, 1982, Cambridge, UK, pp. 93–107. London: The Metals Society.

MOREAU, R. 1980 MHD Flows driven by alternating magnetic fields. In *Proc. 2nd Beer-Sheva Seminar on MHD Flows and Turbulence* (ed. H. Branover & A. Yakhot), pp. 65–82. Israel University Press.

SNEYD, A. 1971 Generation of fluid motion in a circular cylinder by an unsteady applied magnetic field. *J. Fluid Mech.* **49**, 817–827.

SNEYD, A. 1979 Fluid flow induced by a rapidly alternating or rotating magnetic field. *J. Fluid Mech.* **92**, 35–51.

TABERLET, E. & FAUTRELLE, Y. R. 1985 Turbulent stirring in a experimental induction furnace. *J. Fluid Mech.* **159**, 409–431.

TARAPORE, E. D. & EVANS, J. W. 1976 Fluid velocities in induction melting furnaces, part 1: theory and laboratory experiments. *Metall. Trans.* B **7**, 343–351.

TRAKAS, C., TABELING, P. & CHABRERIE, J. P. 1984 Etude experimentale du brassage turbulent dans le four à induction. *J. Méc. Théor. Appl.* **3**, 345–370.